CRYSTAL GROWTH & DESIGN

COMMUNICATION

pubs.acs.org/crystal

Characterization of Structural Changes Associated with Doping Silicon Nanowires by Ion Implantation

Pratyush Das Kanungo,*[,†] Reinhard Koegler,[‡] Nikolai Zakharov,[†] Peter Werner,[†] Roland Scholz,[†] and Wolfgang Skorupa[‡]

[†]Max Planck Institute of Microstructure Physics, Weinberg 2, Halle D-06120, Germany

[‡]Institute of Ion Beam Physics and Materials Research, Forschungszentrum Dresden-Rossendorf e.V., P.O. Box 510119, 01314 Dresden, Germany

Supporting Information

ABSTRACT:

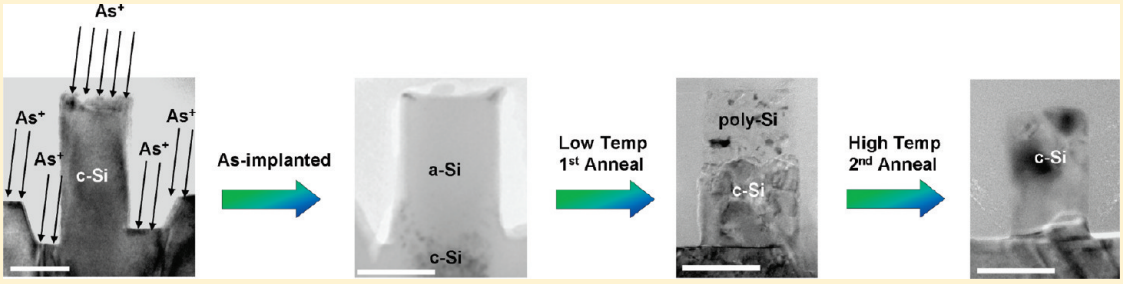

Ion implantation can be a very useful technique to dope silicon nanowires heavily to improve their electrical properties. However, heavy implantation can amorphize the nanowires completely. Subsequently, a complete recovery of their crystallinity, which is of utmost importance to ensure their improved electrical properties, becomes nontrivial. We have performed a controlled study of nanowire recrystallization using vertical Si⟨111⟩ nanowires that were amorphized during doping by arsenic ion implantation. Upon a single-step thermal anneal by furnace (500−650 °C) or by rapid thermal annealing (800−1200 °C), the nanowires turned partly single-crystalline from the bottom and partly polycrystalline from the top, owing to a competition between solid phase epitaxial regrowth from the substrate and random nucleation and growth, probably originating from the free surface. A complete recrystallization of the amorphized nanowires was achieved only after the furnace-annealed nanowires were annealed for a second time at a higher temperature (950−1200 °C). The polycrystalline grains formed during the first anneal were successfully aligned to the ⟨111⟩ direction, leading to a recovery of the single-crystalline structure of the nanowires.

As the scaling of planar metal oxide semiconductor field effect transistors (MOSFETs) is rapidly approaching toward the integration limit imposed by Moore's Law,[1] alternative device architectures for FETs are fast emerging.[2−6] Two of the alternative architectures, as recommended by the international technology roadmap for semiconductors (ITRS),[5] are multigated vertical FETs such as FinFET,[7] and wrap-gated nanowire-FET (NW-FET).[8,9] For both FinFET and NW-FET, the channel consists of a thin (20 nm or less) three-dimensional rectangular or cylindrical pillar. So far, mostly body-doping from the substrate of the Fins[6,7] and in situ doping during the vapor−liquid−solid (VLS) growth of the NWs[8,9] have been used to fabricate the FETs. However, in order to integrate these FETs with the standard CMOS process flow, doping by ion implantation can be a very useful method. On the other hand, heavy implant-doping (dopant concentration $>10^{19}$ cm^{-3}), required for improved electrical properties of these nanostructures, can amorphize them completely and a recovery of their single-crystalline structure can be quite challenging.[10,11]

In order to recover the crystallinity of the structures amorphized by implantation, as well as to electrically activate the dopants, a thermal annealing is required. During annealing, the implanted dopant atoms move to the substitutional lattice sites in the Si crystal in order to be able to accept or donate electrons and contribute to the electrical conductivity. If the annealing temperature is below the silicon melting point, i.e. 1400 °C, it enables solid phase recrystallization of the amorphous silicon (a-Si) via the mechanism of solid phase epitaxial regrowth (SPER),[12−17] wherein the random network of a-Si arranges itself in the same crystal orientation as the substrate underneath, starting from the amorphous−crystalline (a−c) interface. However, in addition to SPER, random nucleation and growth (RNG)[18,19] in the amorphous material can also take place during annealing, seeding from any remaining crystallite in the bulk of the amorphous region, or

Received: January 24, 2011
Revised: May 20, 2011
Published: May 27, 2011

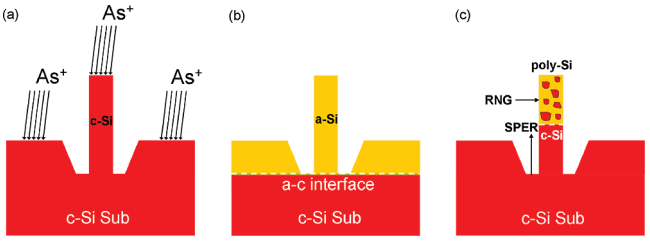

Figure 1. Schematic representation of amorphization by dopant ion implantation and subsequent recrystallization of Si NWs upon a single-step thermal anneal. (a) Implantation of arsenic ions above a critical dose/energy. (b) The resulting fully amorphized NW. (c) The partly crystallized NW after a single-step thermal anneal. The two competing processes, i.e. solid phase epitaxial regrowth (SPER) starting at the a−c interface at the bottom and proceeding upward, and random nucleation and growth (RNG) in the upper volume of the amorphous region, are indicated. This results in the c-Si-poly-Si structure of the NW.

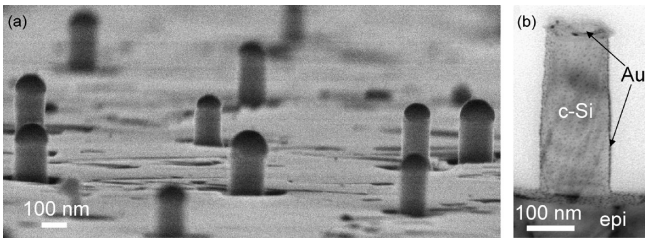

Figure 2. (a) SEM image of as-grown Si NWs. The dark hemispherical caps on top are the solidified remains of the growth-initiating Au droplets. (b) Cross-sectional TEM image (viewed in the ⟨110⟩ zone axis) of a NW with the gold cap removed from the top. The dark spots on the side-walls are the remains of the Au that diffused on the surface while the growth was taking place.

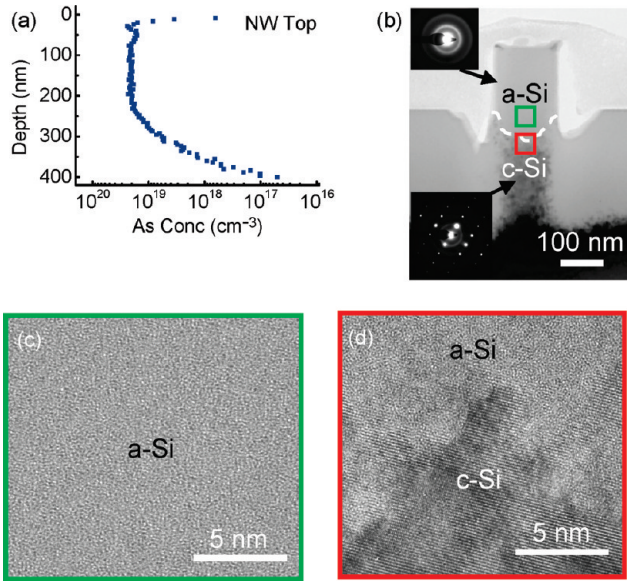

Figure 3. (a) Arsenic implantation profile in the Si NW and the epilayer simulated by TRIM. (b) Cross-sectional TEM image (viewed in the ⟨110⟩ zone axis) of an as-implanted NW. The selected area electron diffraction (SAED) pattern at the top left was taken from the top of the NW, and the same at the bottom left was taken from underneath the NW, i.e. below the a−c interface as indicated. (c) HRTEM image from the bulk of the amorphous region of the NW in part b (green box). (d) HRTEM image from the a−c interface in part b (red box).

even from a defect such as a dangling bond at the Si surface.[18,19] This can particularly happen in these nanostructures (i.e., NWs and FinFETs), which offer a relatively much larger free surface than the two-dimensional devices. It has been shown[10,11] that complete recrystallization of an implanted and amorphized sub-20 nm Fin of a FinFET is heavily affected by RNG. It results in a single-crystalline bottom and a polycrystalline top in the Fin. This phenomenon can also be expected in the case of a Si NW, and the possible transformations of a crystalline NW after implantation are schematically illustrated in Figure 1. The as-implanted NW in Figure 1a may turn completely amorphous (Figure 1b) upon heavy ion implantation (arsenic in this case), and upon a single thermal anneal, it may turn partly single-crystalline and partly polycrystalline (Figure 1c).

Although ion implantation has already been used to dope both horizontal[20,21] and vertical[22−25] Si NWs, a systematic study on the recovery of electrical and structural properties of Si NWs, amorphized by dopant implantation, is lacking in the literature. Following the case of FinFET,[10,11] it can be expected that recrystallization of amorphized NWs will be significantly different from that of amorphized thin films. In this paper, we use ⟨111⟩ oriented vertical Si NWs as a model system to study the NW recrystallization after amorphization by heavy arsenic doping. Arsenic was chosen as the implant specie, since it can act as an n-type dopant as well as can amorphize Si easily, owing to its heavy mass.

The Si NWs used in these experiments were grown by molecular beam epitaxy (MBE) on Si(111) wafers. Au was used to initiate the growth. However, unlike in VLS grown NWs, Au does not act as a growth catalyst, since solid Si, rather than a precursor gas, is used to grow Si NWs in MBE. It was suggested[26] that at the beginning the Au−Si eutectic droplets at the growth temperature (525 °C) establishe a large difference in chemical potential for the incoming Si atoms to incorporate preferentially at the droplets. Subsequently, surface diffusion of Si atoms hitting the base of the NW becomes important.[26] It is worth mentioning that MBE growth of Si NWs using metals other than Au was unsuccessful. Details of the growth process are discussed elsewhere.[26,27] Figure 2a shows scanning electron microscopy (SEM) of as-grown NWs. The NWs were capped with Au hemispheres. In addition, they were decorated with Au nanoparticles on the surface, which are indicated in the transmission electron microscopy (TEM) image in Figure 2b. These Au nanoparticles are remnants of Au that diffused out of the growth-initiating Au droplets on the NW surface. The NW in Figure 2b has its Au cap removed by a wet etching (see Supporting Information). This was done because Au is a heavy atom that can obstruct the penetration of implanted ions into the NW volume. As a result, the average NW height amounted to 300 nm. The as-grown Si NWs were single-crystalline oriented in the ⟨111⟩ direction. In addition to the NW, a parasitic epitaxial layer also grew underneath and around the NW (see Figure 2b).

A four-step multienergy arsenic implantation with the maximum arsenic energy of 300 keV at a dose of 3.32×10^{14} cm^{-2} was carried out to fully amorphize the NWs as well as the surrounding epilayer. This dose is higher than the critical arsenic dose for amorphization in Si[12,13] at 300 keV. All the four implantation energies and doses are listed in Table S1 in the Supporting Information. As shown in Figure 1a, the implantation was done at

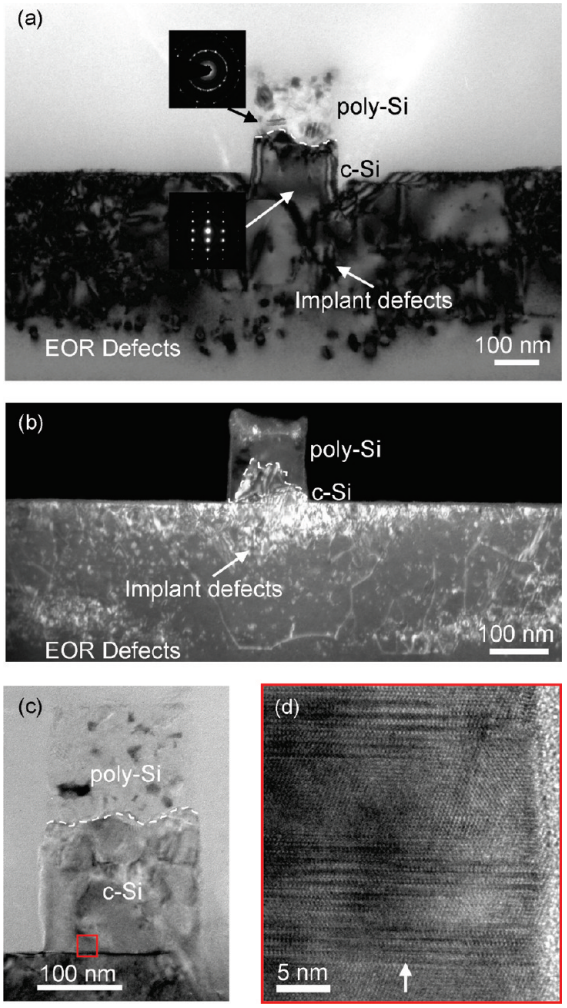

Figure 4. Cross-sectional TEM images (viewed in the ⟨110⟩ zone axis) of Si NWs after a single-step thermal anneal. (a) Overview bright field image after annealing at 550 °C for 5 h in a furnace; top and bottom insets show the SAED patterns taken from above and below the poly-Si−c-Si interface, respectively. It is obvious from the image that the poly-Si appears only in the top part of the NW and not in the epilayer next to the NW, which was equally implanted and amorphized. (b) Overview dark field image of another NW annealed under the same conditions. The implant defects (mainly dislocation loops) are more visible as bright spots in the image. Parts c and d are the overview and HRTEM images (taken from the green box in part c) for another amorphized NW annealed under the same conditions. Part d shows the existence of lamellar twins (indicated with the white arrow) in the c-Si part of the NW.

an angle of 7° in order to avoid ion channeling. In addition, the sample was constantly rotated. The resultant arsenic concentration profile was simulated using the transport of ions in matter (TRIM)[28] code and is shown in Figure 3a. As a result of the four-step implantation, an arsenic concentration of 10^{19} cm^{-3} should be achieved over a depth range of around 300 nm. In order to reduce the self-annealing effect by the ion beam[12,13] and to form a continuous amorphous region in the NW, the implantations were performed at liquid nitrogen temperature (LN_2T).

Figure 3b shows the cross-sectional TEM image of an as-implanted NW. The uniform gray contrast in the entire NW as well as in the epilayer next to it signifies that both of them are indeed fully amorphized. This is further verified with the selected area electron diffraction (SAED) pattern (top left inset) taken from the NW showing the Debye−Scherrer rings typical for amorphous materials. Underneath the NW, a concave shaped a−c interface is visible and is indicated with a dotted line in Figure 3b. For shorter NWs (length ∼200 nm or less), the interface often laid much below (>100 nm) the base of the NW (see Figure S1 in Supporting Information). It is interesting to notice that the a−c interface in the epilayer in Figure 3b is distinctly more flat than that in the NW. This probably results from the shadow effect of the NW as compared to case of the semi-infinite epilayer.[29]

Figure 3c and d show a high resolution TEM image of the NW in Figure 3b taken from the bulk of the amorphous region (green box) and from the a−c interface (red box), respectively. It was verified that although some small crystalline pockets are present at the amorphous side of the a−c interface (see Figure 3d, for example), no such pocket is present in the bulk of the amorphous region (see Figure 3c, for example). This signifies that the amorphization was complete, and no crystalline seeds are left in the amorphous volume of the NW.

In order to study the recrystallization of the fully amorphized NWs, a single-step annealing by two different techniques was performed first. Furnace annealing at 500, 550, 600, and 650 °C for five hours each, as well as rapid thermal annealing (RTA) at 800, 900, 1000, 1050, 1100, and 1200 °C for 30 s each were carried out. All the annealings were performed in argon atmosphere. The annealing conditions are listed in Table S2 in the Supporting Information, and the results are summarized below.

Figure 4a shows an overview TEM cross-sectional image of a NW and the surrounding epilayer after a furnace anneal at 550 °C for 5 h. As confirmed by the SAED pattern at the top and bottom insets in Figure 4a, the top part of the NW is polycrystalline and the bottom part is single-crystalline. The small dark patches in the otherwise gray matrix of the top part are single-crystalline grains. In contrast, the regrown epilayer is fully single-crystalline. As marked in Figure 4a, the end of range (EOR) defects appear at around 300 nm from the surface, marking the original a−c interface. The SPER velocity in Si⟨111⟩ is known to be the slowest,[30] and the regrowth is known to generate crystal defects.[12,13,31] This is obvious from the defective epilayer and the single-crystalline part of the NW. However, it is worth noting that the SPER velocity is unaffected at the implanted concentration of As.[12,13] The implant defects are more clearly visible in the dark-field TEM image of Figure 4b as bright spots. They are mostly dislocation loops formed by agglomeration of point defects created during implantation, upon annealing. Figure 4c shows another NW annealed under similar conditions, and Figure 4d shows an HRTEM image from the bottom part of the NW in Figure 4c. Twin defects are observed and indicated in Figure 4d. Twinning of Si⟨111⟩ has been observed both for SPER of Si thin films[12,13,31] and for VLS growth of Si NWs.[32−34] In the case of NWs, Davidson et al.[32] have termed them as lamellar twins. For recrystallization along the ⟨111⟩ direction, a simultaneous attachment of three adjacent atoms from an amorphous to a crystalline part is required in order to initiate the nucleation. These three atoms can add either in the desired ⟨111⟩ direction or in a twin orientation.

It is worth noting that, unlike the NW, the epilayer did not show any trace of polycrystalline grains. This is the most striking structural difference between the epilayer and the NW. The poly-Si formation in the Si NW results from RNG, as illustrated in Figure 1. The huge surface-to-volume ratio in the NW, as compared to the epilayer, does provide an excess of dangling

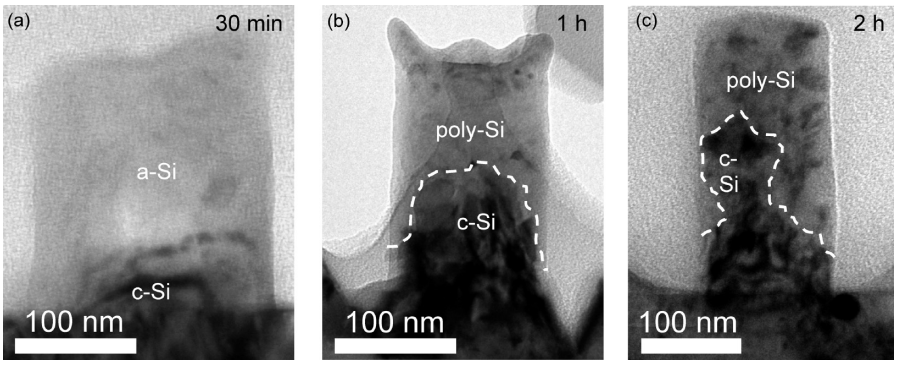

Figure 5. Cross-sectional TEM images (viewed in the ⟨110⟩ zone axis) of fully amorphized Si NWs after a single-step furnace anneal at 550° for different durations: (a) 30 min; (b) 1 h; (c) 2 h.

bonds at the NW surface from where RNG can initiate. In addition, metal induced crystallization[35,36] of Si can also happen locally through the Au nanoparticles on the NW sidewalls (see Figure 2b). A detailed investigation of the role of Au nanoparticles in the poly-Si grain formation is underway. However, the stark difference in the regrown epilayer and the NWs proves that regrowth behavior in a NW is different from that in a thin film.

To estimate the time scale of the starting of RNG in the amorphized Si NWs, furnace annealing at 550 °C was done additionally for three different durations, i.e. 30 min, 1 h, and 2 h. The corresponding TEM images are shown in parts a, b, and c, respectively, of Figure 5. It can be seen that after the 30 min anneal (Figure 5a) SPER merely recrystallizes around 20% of the total length of the NW at the bottom, while the bulk of the NW remains amorphous; that is, the poly-Si formation did not start. However, after an hour of annealing (see Figure 5b) poly-Si already forms at the upper part of the NW, as in case of the 5 h annealing in Figure 4a. The same phenomenon was observed after 2 h of annealing (Figure 5c). In all of the above three cases, SPER recrystallizes around 50% of the total length of the NW from the bottom. Therefore, we conclude that the random nucleation starts in between 30 min and 1 h and no significant improvement on the complete recrystallization can be achieved by annealing them for any longer durations. Similar observations were recorded for all the single-step annealings in a furnace (listed in Table S2 in the Supporting Information). All RTAs at high temperatures (800−1200 °C, see Supporting Information) also resulted in the formation of poly-Si at the top (see Figure S2a in the Supporting Information for an example). This is because the incubation time for poly-Si nucleation is much shorter at higher temperatures. This brings us to the following important conclusions.

If the amorphized NWs are annealed at lower temperatures, the SPER velocity in the NW is slow and RNG sets in beyond 30 min of annealing in a furnace, leading to only partial recovery of the single-crystalline structure of the NWs. On the other hand, if the amorphized NWs are annealed at higher temperatures and for shorter durations, RNG sets in immediately, leading to the similar partially recrystallized structures. The activation energy for SPER in the Si thin film is around 2.7 eV,[12,13] and that for poly-Si nucleation it is 4−5 eV.[18,19] However, we believe that both the activation energies are significantly reduced in the NW, especially that for poly-Si nucleation. This is why it starts even at 500 °C. Therefore, it is clear that a single-step anneal inherently leads to a partly single-crystalline−partly polycrystalline structure

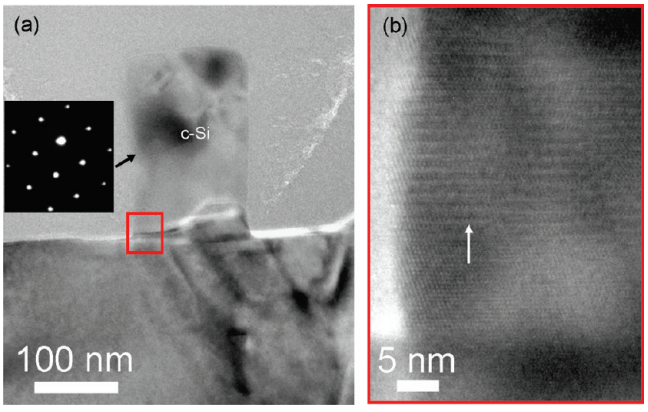

Figure 6. Cross-sectional TEM images (viewed in the ⟨110⟩ zone axis) of a NW after the second anneal at 1100 °C for 1 h in a furnace. (a) Overview image showing that the NW turns completely single-crystalline (see the SAED pattern at the top left taken from the upper-middle part of the NW). (b) HRTEM image taken from the bottom part of the NW. It shows the lamellar twins observed after the first anneal (Figure 4d) still exist at the bottom of the NW.

with a pronounced grain boundary in the middle of the NW. This grain boundary can increase the carrier scattering and deteriorate the electrical properties of the NW, and therefore, it is not desirable.

In order to fully recrystallize the NWs, a reorientation of the grains formed by RNG is necessary. We achieved this by annealing the NWs a second time at a higher temperature (950 °C or above). Figure 6a shows a cross-sectional TEM image of a NW after a first anneal at 550 °C for 5 h followed by a second anneal at 1100 °C for 1 h in a furnace. A striking difference between this NW and the NWs in Figures 4a and 5b and c is the absence of any polycrystalline segment in the upper part of the NW. It is fully single-crystalline (in the ⟨111⟩ direction), which is also corroborated by the SAED pattern taken from the NW. Similar results were obtained for NWs for which the second anneal was done by RTA (see Figure S2b in the Supporting Information). Table S2 in the Supporting Information lists the different combinations of anneals performed in sequence, all of which led to the recovery of the c-Si structure in the NW. This implies that the individual grains observed in Figures 4a and 5b and c are all reoriented in the ⟨111⟩ direction upon the high temperature anneal. In addition, the number of defects in the epilayer reduced drastically for the NW

in Figure 6a (as compared to Figure 4a) due to Ostwald ripening of the smaller defects.[12,13] This recovery of the single-crystalline structure of the NW and removal of the pronounced grain boundary observed in Figures 4a and 5b and c are remarkable. However, the strain field contrast in the NW does indicate the presence of a few dislocation loops. HRTEM imaging from the base of the NW (Figure 6c) also revealed similar lamellar twinning, as observed after the first anneal (see Figure 4d). It shows the relatively high thermal stability of these twins compared to randomly oriented grains. For the use of doped Si NWs in three-dimensional nano-FETs, it is required to avoid out-diffusion of the implanted dopants during annealing. Therefore, we think that RTA rather than furnace annealing is more suitable to achieve complete recrystallization without compromising on dopant activation in the NWs at the second annealing step. This, however, has to be verified with a detailed study of the electrical characterization of the recrystallized NWs, which is underway.

In conclusion, using MBE-grown ⟨111⟩ oriented Si NWs as a model system, we have investigated recrystallization of NWs amorphized by dopant implantation. We have shown that both a low temperature and a high temperature single-step anneal are ineffective in completely recrystallizing an amorphized NW, owing to a competition between SPER and RNG. We have also demonstrated that the single-crystalline structure of the NWs can only be recovered via a sequential anneal comprising a low temperature first anneal and a high temperature second anneal.

■ ASSOCIATED CONTENT

Supporting Information. Details of the wet etching procedure to remove Au from the Si NWs, tables containing key parameters for implantation and annealing, and additional TEM images of amorphized and recrystallized Si NWs. This material is available free of charge via the Internet at http://pubs.acs.org.

■ AUTHOR INFORMATION

Corresponding Author
*E-mail: kanungo@mpi-halle.de.

■ ACKNOWLEDGMENT

The authors would like to dedicate this paper to Ulrich Gösele, the former director of Max Planck Institute of Microstructure Physics, who passed away in November 2009. The authors acknowledge Mrs. Sigrid Hopfe and Mrs. Claudia Münx for preparations of the TEM samples, and Dr. Oussama Moutanabbir and Dr. Viton Heera for useful scientific discussions.

■ REFERENCES

(1) Moore, G. *Electronics* **1965**, *38*, 1959.
(2) Risch, L. *Mater. Sci. Eng: C* **2002**, *19*, 363.
(3) Huff, H. R. *Into the Nano Era*; Springer-Verlag: Berlin, 2009.
(4) Theis, T. N.; Solomon, P. M. *Science* **2010**, *327*, 1600–1601.
(5) International Technology Roadmap for Semiconductors, http://public.itrs.net/reports.html, 2009 edition of Emerging Research Devices.
(6) Wong, H. S. *IBM J. Res. Dev.* **2002**, *46*, 133.
(7) Hisamoto, D.; Lee, W. C.; Kedzierski, J.; Takeuchi, H.; Asano, K.; Kuo, C.; Anderson, E.; King, T. J.; Bokor, J.; Hu, C. *IEEE Trans. Electron Dev.* **2000**, *47*, 2320.
(8) Schmidt, V.; Riel, H.; Senz, S.; Karg, S.; Riess, W.; Gösele, U. *Small* **2005**, *2*, 85.
(9) Goldberger, J.; Hochbaum, A. I.; Fan, R.; Yang, P. *Nano Lett.* **2006**, *6*, 973.
(10) Duffy, R.; Van Dal, M. J. H.; Pawlak, B. J.; Kaiser, M.; Weemaes, R. G. R.; Degroote, B.; Kunnen, E.; Altamirano, E. *Appl. Phys. Lett.* **2007**, *90*, 241912.
(11) Pawlak, B. J.; Duffy, R.; Keersgieter, A. D. *Mater. Sci. Forum* **2008**, *573*, 333.
(12) Rimini, E. *Ion implantation: Basics to device fabrication*; Kluwer Academic Publishers: Boston, 1995.
(13) Nastasi, M.; Mayer, J. W. *Ion implantation and synthesis of materials*; Springer-Verlag: Berlin, 2006.
(14) Lau, S. S. *J. Vac. Sci. Technol.* **1978**, *15*, 1656.
(15) Csepregi, L.; Mayer, J. W.; Sigmon, T. W. *Appl. Phys. Lett.* **1976**, *29*, 92.
(16) Olson, G. L.; Roth, J. A. *Mater. Sci. Rep.* **1988**, *3*, 1.
(17) Narayan, J.; Holland, O. W. *Phys. Status Solidi A* **1982**, *73*, 225.
(18) Köster, U. *Phys. Status Solidi A* **1978**, *48*, 313.
(19) Spinella, C.; Lombardo, S.; Priolo, F. *J. Appl. Phys.* **1998**, *84*, 5383.
(20) Cohen, G. M.; Rooks, M. J.; Chu, O. J.; Laux, S. E.; Solomon, P. M.; Ott, J. A.; Miller, R. J.; Haensch, W. *Appl. Phys. Lett.* **2007**, *90*, 233110.
(21) Colli, A.; Fasoli, A.; Ronning, C.; Pisana, S.; Piscanec, S.; Ferrari, A. C. *Nano Lett.* **2008**, *8*, 2188.
(22) Hoffmann, S.; Bauer, J.; Ronning, C.; Stelzner, T.; Michler, J.; Ballif, C.; Sivakov, V.; Christiansen, S. H. *Nano Lett.* **2009**, *9*, 1341.
(23) Das Kanungo, P.; Koegler, R.; Nguyen-Duc, K.; Zakharov, N. D.; Werner, P.; Gösele, U. *Nanotechnology* **2009**, *20*, 165706.
(24) Das Kanungo, P.; Koegler, R.; Werner, P.; Gösele, U.; Skorupa, W. *Nanoscale Res. Lett.* **2010**, *5*, 243.
(25) Ou, X.; Das Kanungo, P.; Koegler, R.; Werner, P.; Gösele, U.; Skorupa, W.; Wang, X. *Nano Lett.* **2010**, *10*, 171.
(26) Zakharov, N. D.; Werner, P.; Sokolov, L.; Gösele, U. *Physica E* **2006**, *37*, 148.
(27) Werner, P.; Zakharov, N. D.; Gerth, G.; Schubert, L.; Gösele, U. *Int. J. Mater. Res.* **2006**, *97*, 1008.
(28) www.srim.org.
(29) Spaepen, F. *Acta Metall.* **1978**, *26*, 1167.
(30) Csepregi, L.; Kennedy, E. F.; Sigmon, T. W. *J. Appl. Phys.* **1978**, *49*, 3906.
(31) Jones, K. S.; Prussin, S.; Weber, E. R. *Appl. Phys. A: Mater. Sci. Process.* **1988**, *45*, 1.
(32) Davidson, F. M.; Lee, D. C.; Fanfair, D. D.; Korgel, B. A. *J. Phys. Chem. C* **2007**, *111*, 2929.
(33) Conesa-Boj, S.; Zardo, I.; Estradé, S.; Wei, L.; Alet, P. J.; Cabarrocas, P. R. I.; Morante, J. R.; Peiró, F.; Morral, A. F. I.; Arbiol, J. *Cryst. Growth. Des.* **2010**, *10*, 1534.
(34) Arbiol, J.; Morral, A. F. I.; Estradé, S.; Peiró, F.; Kalache, B.; Cabarrocas, P. R. I.; Morante, J. R. *J. Appl. Phys.* **2008**, *104*, 064312.
(35) Yang, R. Y.; Weng, M. H.; Liang, C. T.; Su, Y. K.; Shy, S. L. *Jpn. J. Appl. Phys.* **2006**, *45*, 1146.
(36) Hultman, L.; Robertsson, A.; Hentzell, H. T. G.; Engstrom, I.; Psaras, P. A. *J. Appl. Phys.* **1987**, *62*, 3647.